PERGAMON

Transportation Research Part B 35 (2001) 337–365

TRANSPORTATION RESEARCH PART B

www.elsevier.com/locate/trb

A finite difference approximation of a non-equilibrium traffic flow model

H.M. Zhang *

Civil and Environmental Engineering , University of California at Davis, 156 Everson Hall, Davis, CA 95616, USA

Received 4 January 1999; received in revised form 7 September 1999; accepted 6 October 1999

Abstract

We develop in this paper a finite difference scheme for a previously reported non-equilibrium traffic flow model. This scheme is an extension of Godunov's scheme to systems. It utilizes the solutions of a series of Riemann problems at cell boundaries to construct approximate solutions of the non-equilibrium traffic flow model under general initial conditions. Moreover, the Riemann solutions at both left (upstream) and right (downstream) boundaries of a highway allow the specification of correct boundary conditions using state variables (e.g., density and/or speed) rather than fluxes. Preliminary numerical results indicate that the finite difference scheme correctly computes entropy-satisfying weak solutions of the original model.

Keywords: Finite difference; Riemann problem; Godunov scheme; Traffic flow

1. Introduction

Continuum traffic flow models have found wide applications in areas such as traffic prediction, incident detection and traffic control. Often described by a single or system of nonlinear partial differential equations, these models usually cannot be solved analytically for general initial/boundary conditions. Finite difference schemes are therefore often used to obtain approximate solutions. While a number of good numerical schemes, such as the Lax–Friedrich's scheme and Godunov's scheme, have been developed to solve the scalar kinematic wave model of Lighthill and Whitham (1955) and Richards (1956) (e.g., Michalopoulos et al., 1984; Bui et al., 1992; Daganzo, 1995; Lebacque, 1996), numerical methods for solving higher-order (or non-equilibrium) traffic flow models are less developed (e.g., Leo and Pretty, 1992). Historically, deficient

* Tel.: +1-530-754-9203; fax: +1-530-752-7872.
E-mail address: hmzhang@ucdavis.edu (H.M. Zhang).

0191-2615/01/$ - see front matter
PII: S0191-2615(99)00054-5

numerical schemes (e.g., simple forward/backward difference schemes) were often used to compute approximate solutions of certain higher-order models such as the Payne–Whitham (PW) model (Payne, 1971; Whitham, 1974), and caused confusion over the properties of these models because the mis-behavior of the finite difference schemes was sometimes mistaken as the behavior of the models themselves (e.g., Derzko et al., 1983; Ross, 1988).

A major hindrance to the development of accurate finite difference approximations of higher-order traffic flow models is the lack of a complete understanding of various kinds of waves present in these models. Unlike the kinematic wave model that has only one family of sound, shock and rarefaction waves, higher-order models such as the PW model have two families of such waves (e.g., Zhang, 1999b). Recently, Zhang (1999b) studied the nature of these waves and the occasions in which different kinds of waves arise in both PW model and another higher-order model developed previously by Zhang (1998) (for brevity, hereafter referred to as Zhang's model), and established the solutions of Riemann problems [1] for both models. This work essentially removed the aforementioned hindrance and paved the way for the development of accurate finite difference approximations of a class of higher-order models that include the PW model and Zhang's model.

In this paper we develop a finite difference approximation for Zhang's model based on Godunov's scheme, a finite difference scheme that has been successfully applied to solve the scalar LWR model by a number of researchers (e.g., Bui et al., 1992; Daganzo, 1995; Lebacque, 1996). [2] We organize this paper as follows: we introduce continuum models in Section 2, discuss the basic concepts of finite difference and notions of conservative schemes in Section 3, and develop a Godunov-type scheme for the initial value problem comprising the homogeneous equations of Zhang's model in Section 4. We then extend the Godunov-type finite difference scheme to the full Zhang's model with boundaries in Section 5 and present numerical results in Section 6. Finally, we conclude the paper with a discussion in Section 7.

2. Continuum traffic flow models

Among all continuum traffic flow models, the simplest model is perhaps the kinematic wave model of Lighthill and Whitham (1955) and Richards (1956) (LWR model)

$$\rho_t + f_*(\rho)_x = 0, \tag{1}$$

where ρ and $f_*(\rho)$ are traffic concentration (density) and flux, respectively, and t denotes partial derivative with respect to time, and x the partial derivative with respect to space. Throughout the paper, functions with a subscript $*$, such as f_* and v_*, denote *equilibrium* relations.

The LWR model is a nonlinear *hyperbolic* (see Section 3 for the definition of hyperbolicity) partial differential equation with characteristic (or wave) velocity

$$\lambda_*(\rho) = f'_*(\rho),$$

[1] A Riemann problem refers to a single or system of partial differential equations equipped with a special kind of initial data – Riemann data – that comprises two constant states separated by a single jump.

[2] Both Daganzo's and Lebacque's schemes are streamlined Godunov schemes that are particularly suited for modeling network traffic.

where $'$ is a short hand notation for total derivative d/d. It is customary to assume the flux function $f_*(\rho)$ to be strictly *concave*. Thus in the LWR model waves associated with light traffic travel faster than waves associated with dense traffic. If traffic is dense downstream and light upstream on a road, faster waves carrying light traffic will eventually catch up with slower waves carrying heavy traffic to form a *shock* (i.e., a density/speed jump in space). On the other hand, if traffic is heavy upstream and light downstream, slower upstream waves travel further and further behind the faster downstream waves. This leaves a wider and wider region between slower and faster traffic in which cars accelerate from lower speeds to higher speeds. On the characteristic graph in (x,t) plane this region has a fan-like structure and is often referred to as a *rarefaction wave* fan.

Wave patterns in the LWR model is rather simple: they either comprise shocks, or rarefaction waves or combinations of both, and there is only one kind of shocks and one kind of rarefaction waves. However, traffic flow in the real world often produces much more complex wave patterns, and efforts to model such patterns led to the development of *non-equilibrium* or higher-order continuum models. One class of non-equilibrium continuum models is described by the following system of partial differential equations:

$$\rho_t + (\rho v)_x = 0, \tag{2}$$

$$v_t + v v_x + \frac{c^2(\rho)}{\rho}\rho_x = \frac{v_*(\rho) - v}{\tau}. \tag{3}$$

In this system, τ is the *relaxation time*, v the average travel speed, $v_*(\rho)$ the *equilibrium* travel speed at density ρ ($v_*(\rho) = f_*(\rho)/\rho$, $v_*'(\rho) < 0$), and $c(\rho)$ is *traffic sound speed*. By prescribing different traffic sound speeds, we obtain different traffic models from (2) and (3). For instance, we obtain the PW model if traffic sound speed is chosen to be

$$c(\rho) = \rho_0 v_*'(\rho_0) \equiv c_0 < 0 \tag{4}$$

with ρ_0 suitably chosen to represent prevailing traffic conditions, and Zhang's model if we define traffic sound speed as

$$c(\rho) = \rho v_*'(\rho) < 0. \tag{5}$$

Note that $c(\rho) = f_*'(\rho) - v_*(\rho)$, which is the propagation speed of a small disturbance in equilibrium traffic flow relative to its carrying medium – the moving vehicle stream (Zhang, 1998; Zhang, 1999). In general traffic sound speed varies with density. The PW model fixes the traffic sound speed for all conditions, which is obviously not realistic. [3]

Like the LWR model, the system of (2) and (3) is also hyperbolic. Therefore both shock and rarefaction waves are also present in this non-equilibrium model. Unlike the LWR model, however, this hyperbolic system has two families of characteristics:

[3] The PW model has a number of different versions. In one version its sound speed is $-\sqrt{-v_*'(\rho)/2\tau}$, but it is difficult to interpret what this sound speed means. It is clearly not the sound speed that we have defined, i.e., the relative propagation speed of a small disturbance in equilibrium flow. The constant sound speed is unrealistic, but is at least consistent with this definition. Moreover, our definition of sound speed also provides a way of picking c_0 for the PW model.

$$\lambda_{1,2}(\rho, v) = v \pm c(\rho), \quad \lambda_1 < \lambda_2.$$

Corresponding to each characteristic, there is one family of shock and rarefaction waves, respectively. The waves in the first characteristic field, called 1-shocks and 1-rarefactions, behave much like the shocks and rarefactions in the LWR model. The waves in the second characteristic field, on the other hand, behave quite differently: they travel faster than traffic. Owing to relaxation, however, the second family of waves decay exponentially (Zhang, 1999b).

3. Finite difference approximation of hyperbolic PDEs

To make our exposition self contained, we introduce in this section certain basic notions of finite differences, show how some seemingly reasonable straightforward finite difference procedures fail to work, and describe how such problems can be avoided. Before presenting the concepts of finite differences, it is necessary to make clear what type of partial differential equations (PDEs) that we are dealing with, for different kinds of PDEs warrant different types of finite difference schemes. It turns out that all three traffic models, LWR, PW and Zhang, can be expressed in a compact vector form

$$U_t + A(U)U_x = s(U), \tag{6}$$

where $U(x,t) \in R^n$ is the state of the system. For the LWR model $n = 1$ and

$$U = (\rho), \quad A(U) = (f'_*(\rho)), \quad s(U) = (0)$$

and for both the PW model and Zhang's model $n = 2$, and

$$U = \begin{pmatrix} \rho \\ v \end{pmatrix}, \quad A(U) = \begin{pmatrix} v & \rho \\ c^2(\rho)/\rho & v \end{pmatrix}, \quad s(U) = \begin{pmatrix} 0 \\ (v_*(\rho) - v)/\tau \end{pmatrix}.$$

We say that (6) is hyperbolic if $A(u)$ has real and distinctive eigenvalues $\lambda_i(U)$, $i = 1, \ldots, n$. For convenience of presentation we further sort these distinctive real eigenvalues in ascending order

$$\lambda_1 < \lambda_2 < \cdots < \lambda_n.$$

From Section 1 we know that

$$\lambda_1 = \lambda_* = f'_*(\rho)$$

for LWR model, and

$$\lambda_1 = v + c(\rho) < v - c(\rho) = \lambda_2$$

for PW and Zhang models. Thus all three traffic models are hyperbolic. Our problem is to solve approximately this hyperbolic system (6) with initial data

$$U(x,0) = U_0(x), \quad -L \leqslant x \leqslant L \tag{7}$$

and boundary (flux) data

$$F(U(-L,t)) = Q_-(t), \quad F(U(L,t)) = Q_+(t), \quad t \geqslant 0. \tag{8}$$

To solve this initial/boundary value problem numerically, we divide the time and space domain ($t \geqslant 0$, $-L < x < L$) into a mesh of width $h \equiv \Delta x$ and time increment $k \equiv \Delta t$. The grid points of this mesh are denoted by (x_i, t_j)

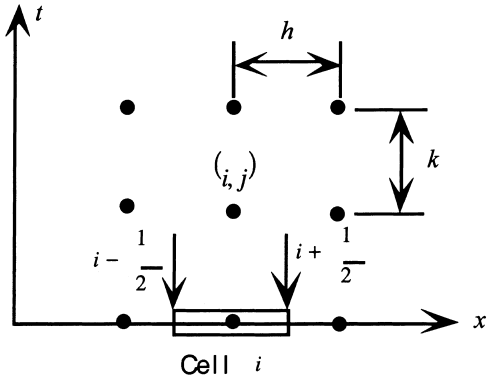

Fig. 1. Finite difference mesh.

$$x_i = ih, \quad i = 0, \pm 1, \pm 2, \ldots, L/h,$$
$$t_j = jk, \quad j = 0, 1, 2, \ldots, T/k$$

with the values of $U(x,t)$ on those grid points denoted by U_i^j (see Fig. 1). The idea of a finite difference scheme is to use those grid point values to calculate approximate partial time and space derivatives

$$[U_t]_i^j \approx D_j(U_i^j, U_i^{j+1}, \ldots, U_i^{j+p})$$

and

$$[U_x]_i^j \approx D_i(U_{i-q}^j, U_{i-q+1}^j, \ldots, U_{i+q}^j)$$

and use them to replace the continuous time and space derivatives in the original PDE to get a discrete system, a system of finite difference equations (FDEs). The vector functions D_j and D_i and their arguments are chosen based on the type of the PDE and the accuracy required for the FDE. For example, a first order accurate approximation only requires two grid points and the functions D_j and D_i usually take one of the following forms:

$$D_j\left(U_i^j, U_i^{j+1}\right) = \frac{U_i^{j+1} - U_i^j}{k} \tag{9}$$

and

$$D_i^f\left(U_i^j, U_{i-1}^j\right) = \frac{U_i^j - U_{i-1}^j}{h} \text{ or} \tag{10}$$

$$D_i^b\left(U_{i+1}^j, U_i^j\right) = \frac{U_{i+1}^j - U_i^j}{h} \text{ or} \tag{11}$$

$$D_i^c\left(U_{i+1}^j, U_{i-1}^j\right) = \frac{U_{i+1}^j - U_{i-1}^j}{2h}. \tag{12}$$

Eq. (9) is often referred to as the Euler difference in time, (10) forward difference, (11) backward difference, and (12) center difference in space. Thus a straightforward Euler time difference and forward space difference approximation of the LWR model would be

$$\frac{\rho_i^{j+1}-\rho_i^j}{k}+f_*'(\rho_i^j)\frac{\rho_i^j-\rho_{i-1}^j}{h}=0. \tag{13}$$

Such straightforward differencing, however, usually does not work for nonlinear hyperbolic PDEs. This is because hyperbolicity implies a certain causal effect: information is propagated along certain directions (characteristic directions) at finite speeds (characteristic velocities). As such, a state of a hyperbolic system at a point in space and time depends on the states of a prior time from not the entire space but only certain regions of that space – the so called region of dependence. Because of this particular nature of dependence in hyperbolic equations, our straightforward difference scheme (13) fails miserably when traffic waves travel upstream (i.e., $f_*'(\rho_i^j)<0$). Moreover, it is well known that in a hyperbolic PDE discontinuities (shocks) in state variables (e.g., density and speed) can develop spontaneously even with smooth initial data (e.g., Lax, 1972; Courant and Friedrichs, 1948), a feature that is notoriously difficult to compute numerically.

The facts that in a hyperbolic system, information propagates along characteristic directions, discontinuities can develop spontaneously, and a discontinuity can either persist or expand and smooth itself out all warrant special care in approximating such systems with finite difference schemes. We want to make sure about three things before using a particular finite difference scheme:

1. it is consistent with the original PDE, i.e., the FDE converges to the PDE when h and k approach 0 (*consistency*),
2. numerical errors introduced by the FDE do not increase over time (*stability*), and
3. its solutions converge to the right solutions of the original PDE when h and k approach 0 (*convergence*).

It turns out that a particular form of hyperbolic PDEs, called the conservative form, is specially suited for developing finite difference schemes that ensure these three properties. A conservative form of (6), for example, is

$$U_t+F(U)_x=s(U). \tag{14}$$

Eq. (14) is called a conservative form because it arises from certain conservative phenomena in convective transport

$$\frac{\partial}{\partial t}\int_L U(x,t)\,\mathrm{d}x+\int_{\partial L}F(U)\,\mathrm{d}x=\int_L s(U)\,\mathrm{d}x. \tag{15}$$

For example, the conservation of vehicles on a finite road segment $L=[x_1,x_2]$ leads to a specific case of (15)

$$\frac{\partial}{\partial t}\int_{x_1}^{x_2}\rho(x,t)\,\mathrm{d}x+(\rho v)(x_2,t)-(\rho v)(x_1,t)=s(\rho,v). \tag{16}$$

Unfortunately, the conservative form of a PDE is not unique. When a hyperbolic PDE is derived from some physical conservation principles (such as conservation of mass and momentum), we can always go back to the original integral conservation law to pick the right conservative form. In non-equilibrium traffic flow, however, we do not have this luxury, because the second equation that describes the evolution of travel speed is not derived from any known conservation principle. In the absence of a conservation principle, the selection of a conservative

form is somewhat arbitrary. But we may develop some heuristic rules, such as simplicity and consistency in a certain sense, to help pick a conservative form and leave the ultimate judgment to experimental verifications. In this spirit, we choose (14) as the conservative form for (2) and (3), with the flux function F given by

$$F(U) = \begin{pmatrix} \rho v \\ v^2/2 + \phi(\rho) \end{pmatrix}, \quad \phi'(\rho) = \frac{c^2(\rho)}{\rho}.$$

We say that a finite difference scheme is *conservative* if it can be written as

$$\frac{U_i^{j+1} - U_i^j}{k} + \frac{\tilde{F}(U_{i+1}^j, U_i^j) - \tilde{F}(U_i^j, U_{i-1}^j)}{h} = \tilde{s}(U_i^j), \tag{17}$$

where $h\tilde{s}$ is the average net influx from sources and sinks of cell i and $\tilde{F}$ is called *numerical flux*. [4] When a finite difference scheme is in conservative form, the condition for consistency is particularly simple. It requires that the numerical flux function satisfies

$$\tilde{F}(U, U) = F(U).$$

Examples of consistent conservative finite difference schemes in traffic flow are the finite difference schemes of Michalopoulos et al. (1984), Daganzo (1995), and Lebacque (1996) in the scalar case (i.e., the LWR model), and the finite difference scheme of Leo and Pretty (1992) in the system case (e.g., the PW model). Examples of non-conservative finite difference schemes are the forward difference scheme discussed earlier for the LWR model, and the finite difference scheme in FREFLOW for the PW model (Payne, 1979).

A consistent, conservative finite difference approximation, if linear, is guaranteed to converge to the correct solution if it meets a stability condition (LeVeque, 1992). This condition, generally referred to as the CFL (Courant–Friedrichs–Lewy) condition, says that the cell advance speed h/k cannot be greater than the maximum absolute characteristic velocity, i.e.,

$$\max \left| \frac{k}{h} \lambda_i \right| \leqslant 1, \quad i = 1, \ldots, n.$$

Although this theorem has not been proven for most nonlinear systems, computational experiences indicate that the CFL condition is sufficient to ensure convergence for a large number of nonlinear systems. Thus we require the CFL condition in all of our finite difference schemes presented hereafter.

It is evident from (17) that a major task of developing a finite difference scheme is to obtain the numerical flux function that satisfies the consistency, stability and convergence properties. Thus far we have not said anything on what this numerical flux function represents in real flow. To interpret this numerical flux function, we need to go back to the integral conservative form and

[4] The argument list of the numerical flux function can involve more than two nodal points, depending on the required accuracy of the finite difference approximation. (17) uses two nodal values to compute its numerical flux and is first order accurate.

reinterpret U_i^j. Suppose that $u(x,t)$ is a weak solution [5] of the integral conservation law (15). We can write (15) as

$$\int_{x_{i-1/2}}^{x_{i+1/2}} u(x,t_{j+1})\,\mathrm{d}x = \int_{x_{i-1/2}}^{x_{i+1/2}} u(x,t_j)\,\mathrm{d}x - \left[\int_{t_j}^{t_{j+1}} F(u(x_{i+1/2},t)\,\mathrm{d}t - \int_{t_j}^{t_{j+1}} F(u(x_{i-1/2},t)\,\mathrm{d}t\right] + \int_{t_j}^{t_{j+1}} \mathrm{d}t \int_{x_{i-1/2}}^{x_{i+1/2}} s(u(x,t))\,\mathrm{d}x, \tag{18}$$

where $i-1/2$ and $i+1/2$ denotes the left and right boundary of cell i (see Fig. 1), respectively. If we interpret U_i^j as the cell average

$$U_i^j = \frac{1}{h}\int_{x_{i-1/2}}^{x_{i+1/2}} u(x,t_j)\,\mathrm{d}x \tag{19}$$

then

$$\tilde{F}(U_{i+1}^j, U_i^j) = \frac{1}{k}\int_{t_j}^{t_{j+1}} F(u(x_{i+1/2},t)\,\mathrm{d}t \tag{20}$$

is the average flux passing through the cell boundary $x_{i+1/2}$ in the time interval (t_j, t_{j+1}), and

$$\tilde{s}(U_i^j)h = \frac{1}{k}\int_{t_j}^{t_{j+1}} \mathrm{d}t \int_{x_{i-1/2}}^{x_{i+1/2}} s(u(x,t))\,\mathrm{d}x$$

is the average net influx from sources (e.g., entries) and sinks (e.g., exits) of cell i during (t_j, t_{j+1}).

There are a number of ways to evaluate the integral of (20), among which Godunov's method is perhaps the most intuitive and instructive. A Godunov scheme solves locally a Riemann problem at each cell boundary for the time interval (t_j, t_{j+1}), using the cell averages U_i^j as initial data. It then pieces together these Riemann solutions at time t_{j+1} and average them using (19) to obtain new initial data for t_{j+2}, and this process is repeated until T/k is reached. The detailed steps to carry out this procedure is described in the next section.

4. A Godunov-type FDE for non-equilibrium traffic flow

In this section we develop a Godunov-type FDE for the initial value problem of the homogeneous equation

$$U_t + F(U)_x = 0, \quad U(x,0) = U_0(x) \tag{21}$$

of the non-equilibrium traffic model. A Godunov-type FDE for the inhomogeneous Eq. (14) with boundary condition (8) and the source term $s(U)$ will be treated in Section 5, using the solutions obtained here.

[5] A weak solution $u(x,t)$ is a solution that satisfies

$$\int_{t\geqslant 0}\int_{-\infty}^{\infty} (u\varphi_t + F(u)\varphi_x + s(u)\varphi)\,\mathrm{d}x\,\mathrm{d}t + \int_{-\infty}^{\infty} u_0(x)\varphi(x,0)\,\mathrm{d}x = 0$$

for any smooth φ with compact support (a space interval with finite length in our case) in $t \geqslant 0$. For example, a shock in the LWR model is a weak solution of $\rho_t + f_*(\rho)_x = 0$.

First we discretize $U_0(x)$ using (19) to obtain cell averages U_i^0. Suppose that we have advanced our computation to t_j with known cell averages U_i^j, and we want to calculate U_i^{j+1}. Define a piecewise constant function $w(x,t_j)$ using cell averages U_i^j as follows:

$$w(x,t_j) = U_i^j \quad \text{if } x_{i-1/2} < x \leqslant x_{i+1/2} \tag{22}$$

then (21) and (22) forms a new initial value problem (with initial time t_j) that yields an exact solution to $U(x,t)$ at time t_{j+1}. Given that (t_j, t_{j+1}) is sufficiently small such that waves generated at each cell boundary do not interact before t_{j+1}, this solution can be obtained through solving a series of Riemann problems at cell boundaries. The smallness of (t_j, t_{j+1}), as it turns out is guaranteed by the CFL condition. These Riemann problems are characterized by the following initial conditions:

$$u_{i+1/2}(x,t_j) = \begin{cases} U_i^j & \text{if } x - x_{i+1/2} < 0, \\ U_{i+1}^j & \text{if } x - x_{i+1/2} > 0, \end{cases} \quad i = 0, \pm 1, \pm 2, \ldots \tag{23}$$

The Riemann solution of (21) and (23) have been obtained by Zhang (1999b). The solution is self-similar and can be expressed in the form of

$$\psi\left(\frac{x - x_{i+1/2}}{t}; U_{i+1}^j, U_i^j\right).$$

These solutions are of eight basic types – 1-shock, 2-shock, 1-rarefaction, 2-rarefaction, and the following combinations: 1-shock and 2-shock, 1-shock and 2-rarefaction, 1-rarefaction and 2-rarefaction, 1-rarefaction and 2-shock. The latter four types are depicted by characteristic diagrams in the time-space plane shown in Fig. 2. $\psi\left(x - x_{i+1/2}/t;\ U_{i+1}^j,\ U_i^j\right)$ is a 1-shock solution if U_{i+1}^j satisfies

$$\text{H1:}\ v - v_i^j = -\sqrt{\frac{2(\rho_i^j - \rho)(\phi(\rho_i^j) - \phi(\rho))}{\rho_i^j + \rho}}, \quad \rho > \rho_i^j, \tag{24}$$

is a 2-shock if U_{i+1}^j satisfies

$$\text{H2:}\ v - v_i^j = -\sqrt{\frac{2(\rho_i^j - \rho)(\phi(\rho_i^j) - \phi(\rho))}{\rho_i^j + \rho}}, \quad \rho < \rho_i^j. \tag{25}$$

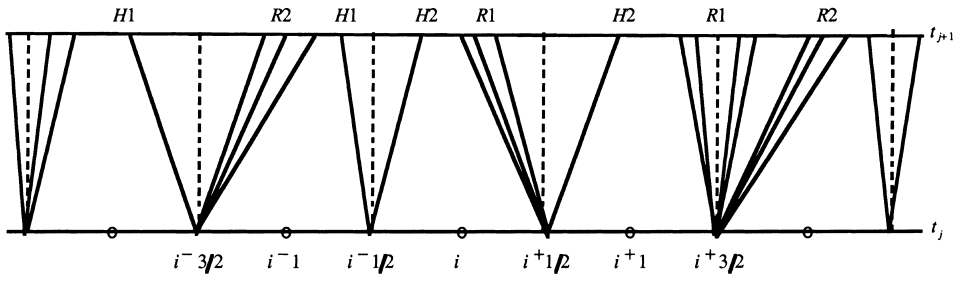

Fig. 2. Riemann solutions at t_{j+1}.

The speed of a 1-shock or 2-shock is given by

$$\sigma = \frac{[\rho v]}{[\rho]}, \tag{26}$$

where [ ] denotes a difference like in $[\rho] = \rho_l - \rho_r$. It is a 1-rarefaction if U_{i+1}^j satisfies

$$\text{R1: } v - v_i^j = v_*(\rho) - v_*(\rho_i^j), \quad \rho < \rho_i^j, \tag{27}$$

and a 2-rarefaction if U_{i+1}^j satisfies

$$\text{R2: } v - v_i^j = v_*(\rho_i^j) - v_*(\rho), \quad \rho > \rho_i^j. \tag{28}$$

There are times when U_{i+1}^j satisfies neither of the four aforementioned phase equations. Under such scenarios the solutions of the Riemann problem in the non-equilibrium model comprise two kinds of waves: a 1-wave (1-shock or 1-rarefaction) and a 2-wave (2-shock or 2-rarefaction). It has been shown that the four phase curves R1, H1, R2 and H2 are all starlike (Zhang, 1999b), therefore for any given point U_i^j in the phase plane, the four phase curves passing through U_i^j divide the phase plane into four quadrants (Fig. 3). We have four possible cases of where U_{i+1}^j would fall into these quadrants, and four types of solutions (Fig. 2).

1-shock + 2-rarefaction: U_{i+1}^j falls in region I. The two waves are separated by a constant state $U_{\mathrm{M}}^{\mathrm{H1R2}}$, to be obtained by solving (24) and (28), with $(\rho_{\mathrm{M}}^{\mathrm{H1R2}}, v_{\mathrm{M}}^{\mathrm{H1R2}})$ replaces (ρ, v) in (24) and (ρ_i^j, v_i^j) in (28).

1-rarefaction + 2-rarefaction: U_{i+1}^j falls in region II. The two waves are separated by a constant state $U_{\mathrm{M}}^{\mathrm{R1R2}}$, to be obtained by solving (27) and (28), with $(\rho_{\mathrm{M}}^{\mathrm{R1R2}}, v_{\mathrm{M}}^{\mathrm{R1R2}})$ replaces (ρ, v) in (27) and (ρ_i^j, v_i^j) in (28).

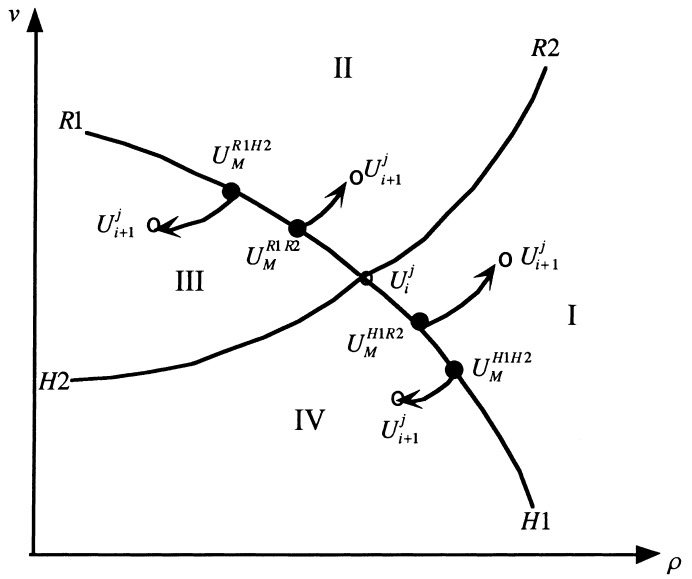

Fig. 3. Riemann solutions on the phase plane.

1-rarefaction + 2-shock: U_{i+1}^j falls in region III. The two waves are separated by a constant state $U_{\mathrm{M}}^{\mathrm{R1H2}}$, to be obtained by solving (27) and (25), with $(\rho_{\mathrm{M}}^{\mathrm{R1H2}}, v_{\mathrm{M}}^{\mathrm{R1H2}})$ replaces (ρ, v) in (27) and (ρ_i^j, v_i^j) in (25).

1-shock + 2-shock: U_{i+1}^j falls in region IV. The two waves are separated by a constant state $U_{\mathrm{M}}^{\mathrm{H1H2}}$, to be obtained by solving (24) and (25), with $(\rho_{\mathrm{M}}^{\mathrm{H1H2}}, v_{\mathrm{M}}^{\mathrm{H1H2}})$ replaces (ρ, v) in (24) and (ρ_i^j, v_i^j) in (25).

Because $\psi(x - x_{i+1/2}/t;\ U_{i+1}^j,\ U_i^j)$ is self-similar and U is constant along characteristics in the homogeneous problem, $U(x_{i+1/2}, t)$ is constant during interval $[t_j, t_{j+1}]$ regardless of the kinds of solutions we obtain. We denote this constant as $U_{i+1/2}^{*j}$. Now our numerical flux $\tilde{F}(U_{i+1}^j, U_i^j)$ becomes

$$\tilde{F}(U_{i+1}^j, U_i^j) = F\left(U_{i+1/2}^{*j}\right), \tag{29}$$

and the Godunov FDE for the homogeneous Zhang's model reads

$$\frac{U_i^{j+1} - U_i^j}{k} + \frac{F\left(U_{i+1/2}^{*j}\right) - F\left(U_{i-1/2}^{*j}\right)}{h} = 0. \tag{30}$$

What is left of the procedure is to obtain $U_{i+1/2}^{*j}$. This can be achieved through solving a series of algebraic, albeit generally highly nonlinear phase equations. Examining the Riemann solution at $x_{i+1/2}$ in detail, we come up with nine cases for $U_{i+1/2}^{*j}$, all listed in Table 1. Traffic conditions (e.g., $U_i^j,\ U_{i+1}^j$) that leads to these nine cases are depicted in Figs. 4–7. Among these values of $U_{i+1/2}^{*j}$, U_i^j and U_{i+1}^j are given, and we know how to obtain $U_{\mathrm{M}}^{*\mathrm{H1R2}}$, $U_{\mathrm{M}}^{*\mathrm{R1R2}}$, $U_{\mathrm{M}}^{*\mathrm{H1H2}}$ and $U_{\mathrm{M}}^{*\mathrm{R1H2}}$. To complete the FDE, we shall next describe how to obtain $U_i^{*\mathrm{R1}}$, $U_i^{*\mathrm{R1H2}}$ and $U_i^{*\mathrm{R1R2}}$.

Let us denote an arbitrary state within a 1-rarefaction fan as $U = (\rho, v)$, and the state on the right edge of the fan as $U_r = (\rho_r, v_r)$. Then the phase equation of a 1-rarefaction wave that spans (U_i^j, U_r) becomes

$$\mathrm{R1}:\ v - v_i^j = v_*(\rho) - v_*(\rho_i^j), \quad \rho < \rho_i^j. \tag{31}$$

Table 1
Obtaining $U_{i+1/2}^{*j}$ from Riemann solutions

Cases	$U_{i+1/2}^{*j}$
1	U_i^j
2	U_{i+1}^j
3	$U_i^{*\mathrm{R1}}$
4	$U_i^{*\mathrm{R1H2}}$
5	$U_i^{*\mathrm{R1R2}}$
6	$U_{\mathrm{M}}^{*\mathrm{H1R2}}$
7	$U_{\mathrm{M}}^{*\mathrm{R1R2}}$
8	$U_{\mathrm{M}}^{*\mathrm{H1H2}}$
9	$U_{\mathrm{M}}^{*\mathrm{R1H2}}$

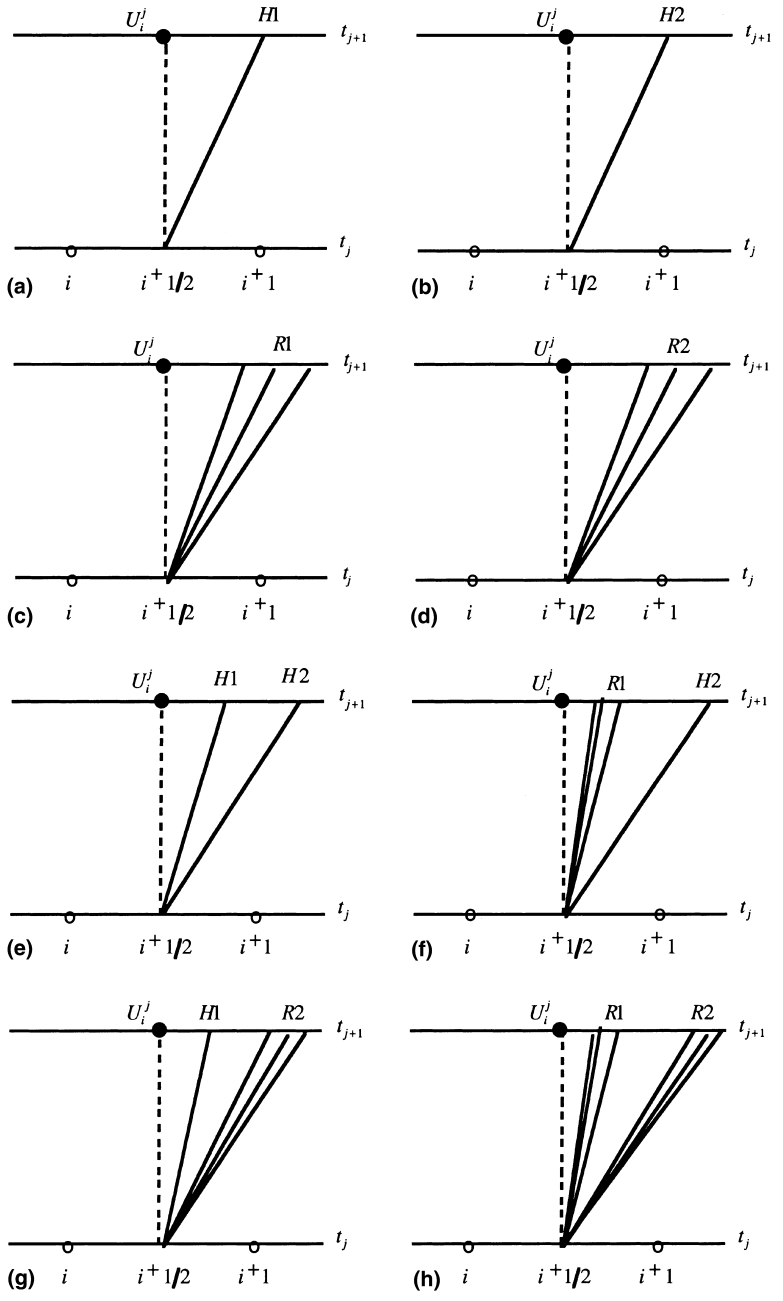

Fig. 4. Traffic conditions that lead to Case 1.

Furthermore, the characteristic originated from (i,j) and passing through $(i,j+1)$ has zero speed:

$$\lambda_1\left(\rho^*\left(\frac{x-x_{i+1/2}}{t}\right), v^*\left(\frac{x-x_{i+1/2}}{t}\right)\right) = \frac{x-x_{i+1/2}}{t} = 0,$$

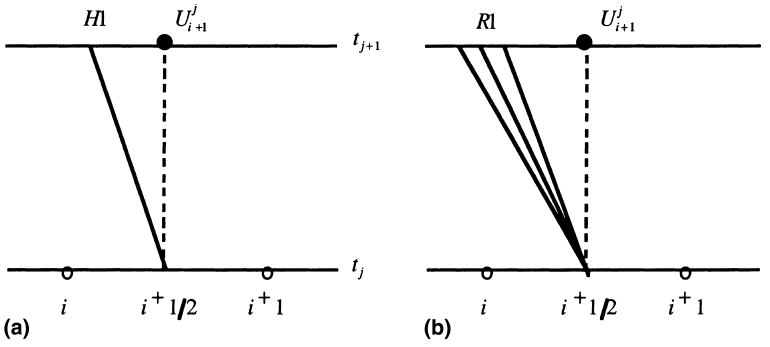

Fig. 5. Traffic conditions that lead to Case 2.

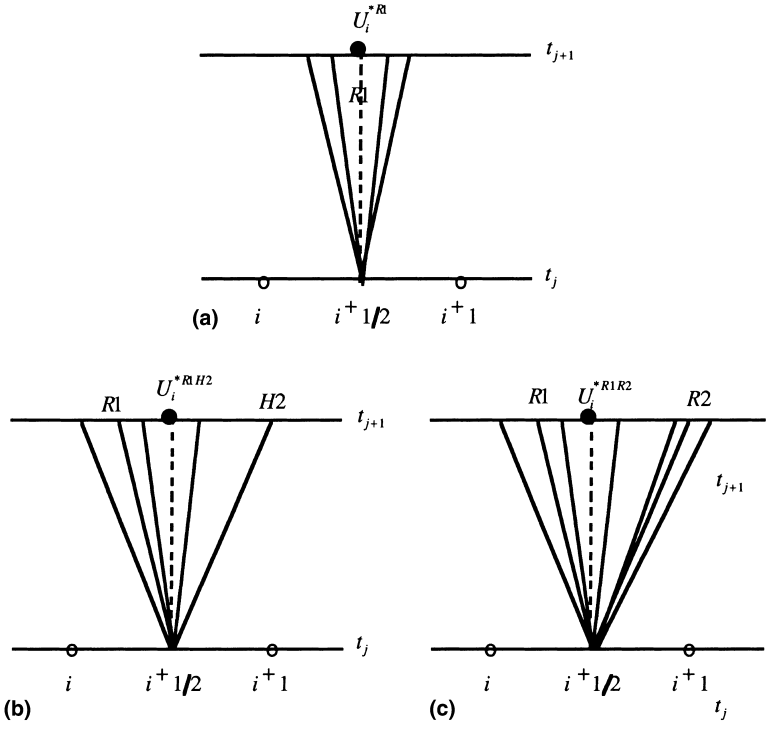

Fig. 6. Traffic conditions that lead to Cases 3–5.

which implies that

$$\begin{aligned}\lambda_1 &= v^* + \rho^* v'_*(\rho^*) \\ &= v_i^j + v_*(\rho^*) - v_*(\rho_i^j) + \rho^* v'_*(\rho^*) \\ &= [v_i^j - v_*(\rho_i^j)] + f'_*(\rho^*) \\ &= 0\end{aligned}$$

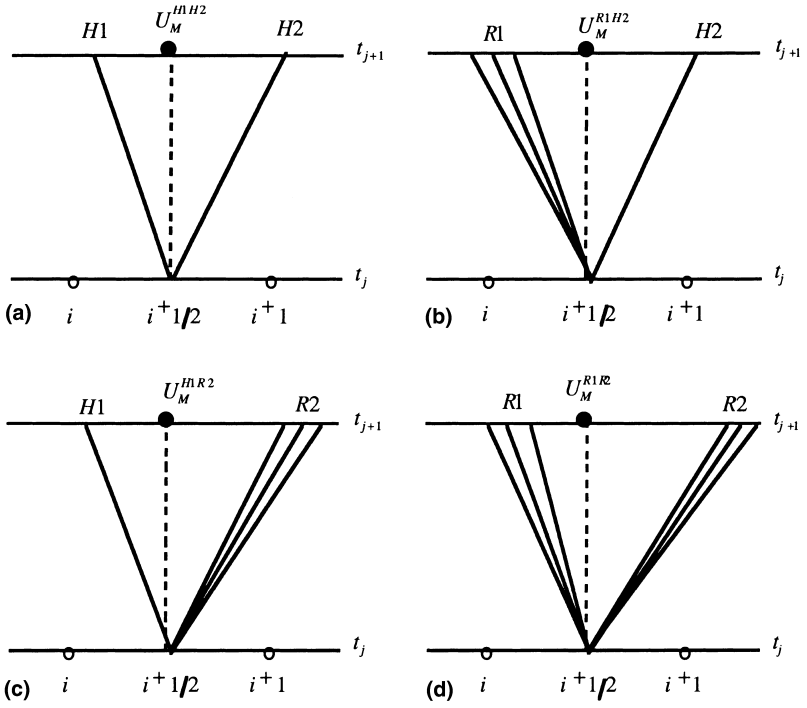

Fig. 7. Traffic conditions that lead to Cases 6–9.

or

$$f'_*(\rho^*) = v_*(\rho_i^j) - v_i^j \equiv \Delta v_i^j. \tag{32}$$

We therefore have

$$\rho^* = (f'_*)^{-1}(\Delta v_i^j), \tag{33}$$

$$v^* = v_*(\rho^*) - \Delta v_i^j. \tag{34}$$

Formulas (33) and (34) can be represented graphically through the flow–density diagram. ρ^* is determined by finding the tangential line of $f_*(\rho)$ whose slope is Δv_i^j. Because $f_*(\rho)$ is concave, there is only one ρ^* corresponding to every tangent of $f_*(\rho)$ (Fig. 8).

Because (ρ^*, v^*) is determined solely by U_i^j and the equilibrium speed v_*, the right state U_r does not come into Eqs. (33) and (34). Thus

$$U_i^{*\mathrm{R1}} = U_i^{*\mathrm{R1H2}} = U_i^{*\mathrm{R1R2}} = (\rho^*, v^*).$$

It should be noted that we never considered cases where a 2-shock or a 2-rarefaction crosses over to the left of the line $\{x(t) : x = x_{i+1/2}\}$. This is because 2-shocks and 2-rarefactions only travel forward, guaranteed by $\lambda_2(U) = v - \rho v'_*(\rho) > v \geqslant 0$ and the entropy conditions that screen out physical weak solutions (Zhang, 1999b).

Another point worth noting is that the FDE for the non-equilibrium model reduces to the Godunov-type FDE of the LWR model in the special case of U_{i+1}^j falling on either a 1-rarefaction

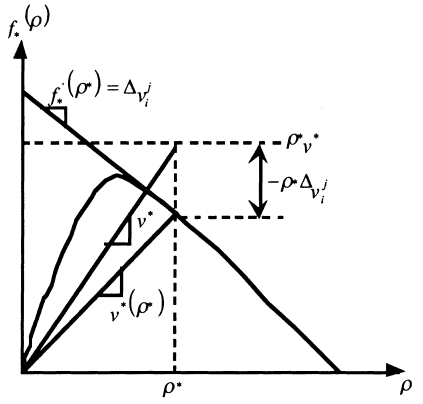

Fig. 8. Graphical representation of (33) and (34).

or a *weak* 1-shock curve originated from U_{i+1}^j , and $v_i^j = v_*(\rho_i^j)$. Under this scenario we have only five cases of $U_{i+1/2}^{*j}$: Figs. 4(a), 5(a), 4(c), 5(b) and 6(a), with

$$\rho^* = (f_*')^{-1}(0), \tag{35}$$

$$v^* = v_*(\rho^*), \tag{36}$$

(see Fig. 9) and a simplified 1-rarefaction curve

$$\text{R1}: \; v = v_*(\rho), \quad \rho < \rho_i^j, \tag{37}$$

and a 1-shock curve

$$\text{H1}: \; v = v_*(\rho_i^j) - \sqrt{\frac{2(\rho_i^j - \rho)(\phi(\rho_i^j) - \phi(\rho))}{\rho_i^j + \rho}}, \quad \rho > \rho_i^j. \tag{38}$$

Note that (37) is precisely the equilibrium speed–density curve, but (38) in general differs from $v_*(\rho)$ unless either $v_*(\rho)$ is linear or ρ and ρ_i^j is sufficiently close: $\rho/\rho_i^j \sim 1$, i.e., a weak 1-shock.

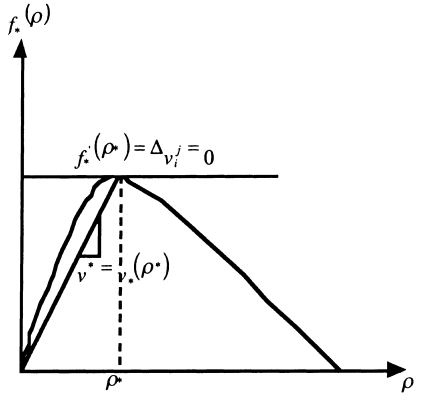

Fig. 9. Graphical representation of (35) and (36).

That (38) reduces to $v = v_*(\rho)$ when $v_*(\rho)$ is linear is obvious. Here we will look only at the case of a weak shock. A weak shock allows a first order Taylor series approximation of $\phi(\rho)$ around ρ_i^j:

$$\phi(\rho) \sim \phi(\rho_i^j) + \phi'(\rho_i^j)(\rho - \rho_i^j), \quad \phi'(\rho_i^j) = \rho_i^j (v_*'(\rho_i^j))^2.$$

Moreover,

$$\frac{2\rho_i^j}{\rho_i^j + \rho} \sim 1.$$

Thus the left-hand side of (38) can be approximated by

$$v_*(\rho_i^j) - \sqrt{\frac{2\rho_i^j}{\rho_i^j + \rho} \left(v_*'(\rho_i^j)(\rho_i^j - \rho)\right)^2} \approx v_*(\rho_i^j) \approx v_*(\rho),$$

and we have

$$\text{H1: } v = v_*(\rho), \ \ \rho > \rho_i^j, \ \ \rho \sim \rho_i^j \tag{39}$$

for a weak 1-shock.

With (37) and (39), (30) reduces to

$$\frac{\rho_i^{j+1} - \rho_i^j}{k} + \frac{f_*(\rho_{i+1/2}^{*j}) - f_*(\rho_{i-1/2}^{*j})}{h} = 0, \quad v_i^{j+1} = v_*(\rho_i^{j+1}) \tag{40}$$

and $\rho_{i+1/2}^{*j}$ is obtained according rules of Cases 1–3 in Table 1. These rules yield a simple formula for $f_*\left(\rho_{i+1/2}^{*j}\right)$:

$$f_*\left(\rho_{i+1/2}^{*j}\right) = \begin{cases} \min_{\rho_i^j \leqslant \rho \leqslant \rho_{i+1}^j} f_*(\rho) & \text{if } \rho_i^j < \rho_{i+1}^j, \\ \max_{\rho_i^j \geqslant \rho \geqslant \rho_{i+1}^j} f_*(\rho) & \text{if } \rho_i^j > \rho_{i+1}^j, \end{cases}$$

which is none other than the Osher formula for scalar conservation laws with a concave flux function (LeVeque, 1992). FDE (40) with Osher formula is the Godunov scheme for the LWR model. This result attests to a certain degree, the consistency between the non-equilibrium model and the equilibrium LWR model, and between their corresponding Godunov-type FDEs.

5. Treatment of boundary conditions and source terms

The source term, $s(U) = (0, (v_*(\rho) - v)/\tau)$, does not involve spatial gradients and therefore does not blow-up as terms on the left-hand side of (17) do. One can simply use $s(U_i^j)$ or $s(U_{i-1}^j + U_{i+1}^j/2)$ to approximate it. Problem of numerical instability may arise, however, when the source term is stiff, i.e., τ is small. Under such situations, we may use a smaller time increment $k \ll \tau$ or a more stable time-difference scheme, such as implicit time difference, to cure this problem.

The proper treatment of boundary conditions, on the other hand, is more involved. Let us start with the simplest case – the scalar LWR model – to show the essential ideas and then extend them to those of systems of traffic flow dynamics. Following Daganzo (1995), we define for each cell a

(concave) sending and a (concave) receiving flux function, or a demand and a supply function as called by Lebacque (1996):

$$\text{Demand: } D(i,j) = \begin{cases} f_*(\rho_i^j) & \text{if } \rho_i^j < \rho^*, \\ f(\rho^*) & \text{if } \rho_i^j \geqslant \rho^*, \end{cases} \tag{41}$$

$$\text{Supply: } S(i,j) = \begin{cases} f_*(\rho_i^j) & \text{if } \rho_i^j > \rho^*, \\ f(\rho^*) & \text{if } \rho_i^j \leqslant \rho^*, \end{cases} \tag{42}$$

where ρ^* is the critical density at which $f'_*(\rho^*) = 0$ (Fig. 10). Furthermore, note that in (40) only the boundary flux $f_*(\rho^{*j}_{1/2})$ (left boundary) and $f_*(\rho^{*j}_{n+1/2})$ (right boundary) enter the FDE at the boundary cells, one therefore can impose an influx f^j_{*-} at the left boundary and an outflux f^j_{*+} at the right boundary. The amount of traffic that wishes to enter cell 1 is f^j_{*-}, and the amount of traffic that can be accommodated downstream of cell n is f^j_{*+}. Physically a cell cannot take in more traffic than it could handle, therefore the actual (realizable) flux passing through both boundaries are given by

$$f_*(\rho^{*j}_{1/2}) = \min\{f^j_{*-}, S(1,j)\}, \tag{43}$$

$$f_*(\rho^{*j}_{n+1/2}) = \min\{D(n,j), f^j_{*+}\}, \tag{44}$$

which are the correct boundary conditions for the LWR model.

This treatment of boundary conditions for the scalar LWR model, although elegant, is ambiguous for the following reason: with a concave flux function there are in general two solutions to $f_*(\rho) = f_{*\alpha}$ (ρ_u and ρ_o in Fig. 10). Formulas (43) and (44) therefore contain an implicit assumption: traffic density (that produces $f_{*\alpha}$) is undercritical ($\rho_u < \rho^*$) for the left boundary and overcritical ($\rho_o > \rho^*$) for the right boundary. Otherwise the demand at the left boundary and the supply at the right boundary could be $f_*(\rho^*)$ and the boundary conditions would be

$$f_*(\rho^{*j}_{1/2}) = \min\{f_*(\rho^*), S(1,j)\}, \tag{45}$$

$$f_*(\rho^{*j}_{n+1/2}) = \min\{D(n,j), f_*(\rho^*)\}. \tag{46}$$

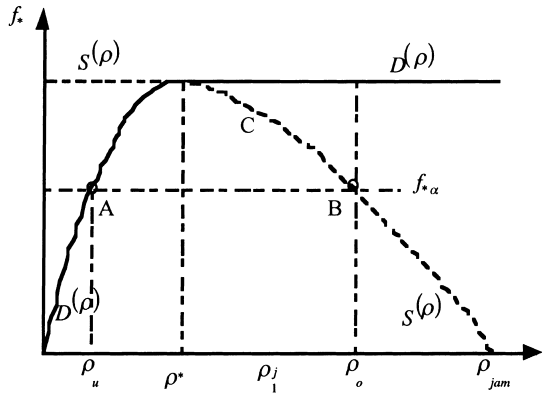

Fig. 10. Supply and demand functions of a cell.

This ambiguity also exists in the non-equilibrium model if we specify boundary flux Q_ρ and Q_v, because the solution of

$$\rho v = Q_\rho, \tag{47}$$

$$\frac{v^2}{2} + \phi(\rho) = Q_v \tag{48}$$

is generally not unique. To see this we substitute $v = Q_\rho/\rho$ into (48) and define

$$g(\rho) = \frac{Q_\rho^2}{2\rho^2} + \phi(\rho),$$

whose derivative

$$g'(\rho) = -\frac{Q_\rho^2}{\rho^3} + \rho(v_*')^2(\rho)$$

vanishes when

$$\rho^2 v_*'(\rho) = -Q_\rho. \tag{49}$$

At those points where $g'(\rho)$ vanishes

$$\begin{aligned} g''(\rho) &= \frac{3Q_\rho^2}{\rho^4} + (v_*')^2(\rho) + 2\rho v_*'(\rho) v_*''(\rho) \\ &= 4(v_*')^2(\rho) + 2\rho v_*'(\rho) v_*''(\rho) \\ &= 2v_*'(\rho)(2v_*'(\rho) + \rho v_*''(\rho)) \\ &= 2v_*'(\rho) f_*''(\rho) \\ &> 0. \end{aligned}$$

That is, $g(\rho)$ is locally strictly convex in the neighborhood of these critical points ρ_c and any Q_v close to $g(\rho_c)$ would yield, in a small neighborhood of ρ_c, either no solution or two solutions to the equation

$$g(\rho) = Q_v.$$

The aforementioned ambiguity, owing to the nature of the flux functions, can be removed if we specify boundary conditions using state variables, such as ρ in LWR and (ρ, v) in Zhang, because a state of traffic flow produces a unique flux. Let $\rho_\pm^j$, $j = 0, 1, \ldots, T/k$ be the right/left boundary data for the the LWR model, and denote the Riemann solutions of the LWR model with initial data (ρ_-^j, ρ_1^j) and (ρ_n^j, ρ_+^j) as $\psi_-(x - x_{1/2}/t;\ \rho_-^j,\ \rho_1^j)$ and $\psi_+(x - x_{n+1/2}/t;\ \rho_n^j,\ \rho_+^j)$, respectively. The boundary fluxes are then uniquely determined by $\psi_\pm$

$$f_*(\rho_{1/2}^{*j}) = f_*\big(\psi_-\big(0; \rho_-^j, \rho_1^j\big)\big), \tag{50}$$

$$f_*(\rho_{n+1/2}^{*j}) = f_*\big(\psi_+\big(0; \rho_n^j, \rho_+^j\big)\big). \tag{51}$$

This way of obtaining boundary fluxes for the scalar LWR model can easily be extended to Zhang's model with boundary data $U_{\pm}^{j},\ j = 0, 1, \ldots, T/k$

$$F(U_{1/2}^{*j}) = F\left(\psi_{-}^{z}\left(0; U_{-}^{j}, U_{1}^{j},\right)\right), \tag{52}$$

$$F(U_{n+1/2}^{*j}) = F\left(\psi_{+}^{z}\left(0; U_{n}^{j}, U_{+}^{j}\right)\right), \tag{53}$$

where Riemann solutions $\psi_{\pm}^{z}$ are obtained in the same way as discussed in Section 4.

6. Numerical examples

In this section we use the developed finite difference scheme to compute the numerical solutions for a number of Riemann problems of both the LWR model and Zhang's model. Since our main objective here is to validate the numerical scheme, we use the special linear flow–density relation $v_*(\rho) = v_0 + b\rho,\ b < 0$ in our calculations. With such a relation, explicit formulas for $U_{i\pm1/2}^{*j}$ can be obtained through a series of coordinate transformations in the (ρ, v) phase plane, and the numerical results can be interpreted more easily.

Remember that for any pair of constant states (U_l, U), different kinds of waves arise depending on which quadrant the right state U falls in the (ρ, v) phase plane. One has to solve a complicated system of algebraic equations to determine the location of U in the phase plane if $v_*(\rho)$ is non-linear. When $v_*(\rho)$ is linear, however, this becomes very straightforward: one simply does two coordinate transformations to locate U in the new phase plane.

First, we shift the origin of (ρ, v) coordinates to U_l. Every U in the new coordinate system becomes $\hat{U} = (\hat{\rho}, \hat{v}) = U - U_l$, whose unit vectors are denoted as $(\hat{\mathbf{e}}_1, \hat{\mathbf{e}}_2)$. Next we rotate the $\hat{\rho},\ \hat{v}$ axes to coincide with the shock and rarefaction phase curves passing through U_l to obtain a new coordinate system $(\tilde{\rho}, \tilde{v})$ (its unit vectors are denoted as $(\tilde{\mathbf{e}}_1, \tilde{\mathbf{e}}_2)$). In this new coordinate system, a one-shock can be represented by $h_1\tilde{\mathbf{e}}_1$, a 2-shock by $-h_2\tilde{\mathbf{e}}_2$, a 1-rarefaction by $-r_1\tilde{\mathbf{e}}_1$, and a 2-rarefaction by $r_2\tilde{\mathbf{e}}_2$, where the scalar constants $h_1, h_2,\ r_1$ and r_2 represent the strength of the shock and rarefaction waves in the new units (Fig. 11).

The unit vectors $\tilde{\mathbf{e}}_1$ and $\tilde{\mathbf{e}}_2$ of the $(\tilde{\rho}, \tilde{v})$ coordinates can be expressed by the unit vectors $(\hat{\mathbf{e}}_1, \hat{\mathbf{e}}_2)$ of the $(\hat{\rho}, \hat{v})$ coordinates

$$\tilde{\mathbf{e}}_1 = \frac{1}{\sqrt{1+b^2}}\hat{\mathbf{e}}_1 + \frac{b}{\sqrt{1+b^2}}\hat{\mathbf{e}}_2, \tag{54}$$

$$\tilde{\mathbf{e}}_2 = \frac{1}{\sqrt{1+b^2}}\hat{\mathbf{e}}_1 + \frac{-b}{\sqrt{1+b^2}}\hat{\mathbf{e}}_2 \tag{55}$$

whose inverse transform is

$$\hat{\mathbf{e}}_1 = \frac{\sqrt{1+b^2}}{2}\tilde{\mathbf{e}}_1 + \frac{\sqrt{1+b^2}}{2}\tilde{\mathbf{e}}_2, \tag{56}$$

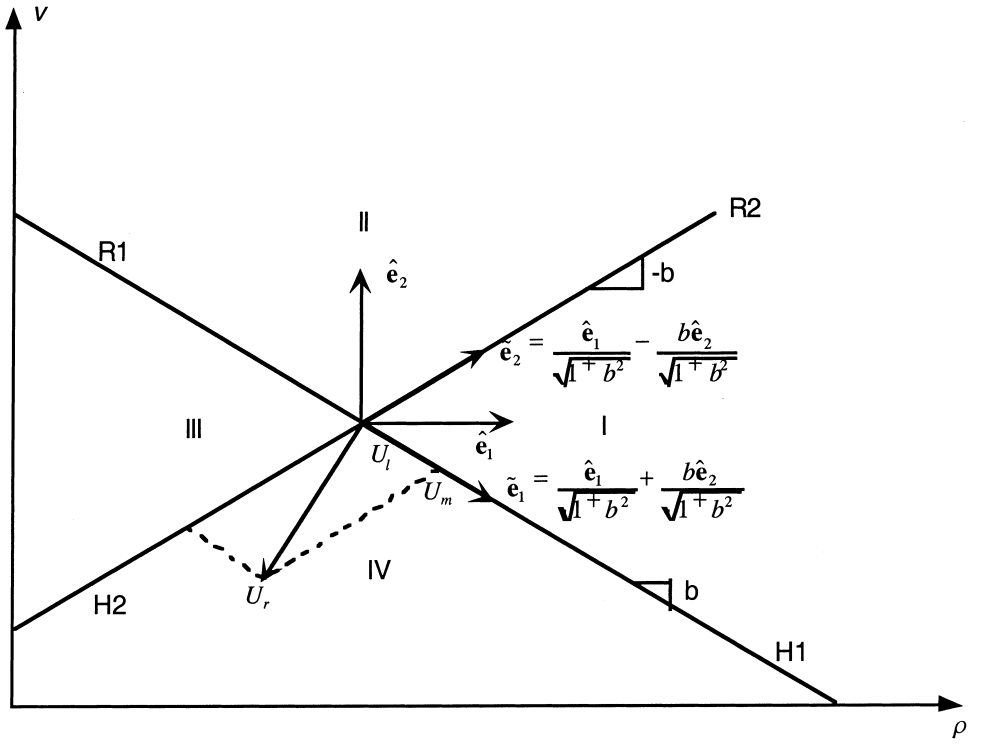

Fig. 11. Coordinate transform in the phase plane.

$$\hat{\mathbf{e}}_2 = \frac{\sqrt{1+b^2}}{2b}\tilde{\mathbf{e}}_1 - \frac{\sqrt{1+b^2}}{2b}\tilde{\mathbf{e}}_2. \tag{57}$$

For any point $\hat{U}$ in the $(\hat{\rho}, \hat{v})$ phase plane, its representation in the $(\tilde{\rho}, \tilde{v})$ phase plane is

$$\hat{U} = (\hat{\rho}, \hat{v}) = \begin{pmatrix} \hat{\rho} & \hat{v} \end{pmatrix} \begin{pmatrix} \hat{\mathbf{e}}_1 \\ \hat{\mathbf{e}}_2 \end{pmatrix} = \frac{\sqrt{1+b^2}}{2}\left(\left(\hat{\rho} + \frac{\hat{v}}{b}\right)\tilde{\mathbf{e}}_1 + \left(\hat{\rho} - \frac{\hat{v}}{b}\right)\tilde{\mathbf{e}}_2\right). \tag{58}$$

Thus the quadrant that $\hat{U}$ falls on $(\tilde{\rho}, \tilde{v})$ can be easily determined based on $\hat{\rho} + (\hat{v}/b)$ and $\hat{\rho} - (\hat{v}/b)$. The results are listed in Tables 2 and 3.

Table 2
Position of $\tilde{U}$ in the $(\tilde{\rho}, \tilde{v})$ phase plane

Quadrant	$\hat{\rho} + (\hat{v}/b)$	$\hat{\rho} - (\hat{v}/b)$
I	> 0	> 0
II	< 0	> 0
III	< 0	< 0
IV	> 0	< 0

Table 3
$\tilde{U}$ falls on shock or rarefaction curves

Waves	$\hat{\rho}+(\hat{v}/b)$	$\hat{\rho}-(\hat{v}/b)$
H1	>0	$=0$
R2	$=0$	>0
H2	$=0$	<0
R1	<0	$=0$

What we are interested in are the intermediate state, which is always on either $\tilde{\mathbf{e}}_1$ or $-\tilde{\mathbf{e}}_1$, i.e.,

$$\tilde{U}_m = \left(\frac{\sqrt{1+b^2}}{2} \left(\hat{\rho} + \frac{\hat{v}}{b} \right), 0 \right). \tag{59}$$

This intermediate state can be transformed back into the (ρ, v) coordinates by an inverse transform, and the result is

$$U_m = \left(\rho_l + \frac{1}{2} \left(\hat{\rho} + \frac{\hat{v}}{b} \right), v_l + \frac{b}{2} \left(\hat{\rho} + \frac{\hat{v}}{b} \right) \right). \tag{60}$$

These formulas, together with the scalar Godunov scheme for the LWR model, were programmed to compute the solutions of six Riemann problems of both models. The initial data for these Riemann problems and the types of waves arising from them are listed in Table 4. Cases 1 and 2 provide a check to the validity of our proposed finite difference scheme because in theory the solutions of both Zhang's model and the LWR model (with a linear $v_*(\rho)$) are identical with these set of initial conditions. The other cases were selected to demonstrate the similarities and differences of solutions between the two models.

The numerical solutions (i.e., density and speed over space and time) corresponding to the six set of initial data are depicted in Figs. 12–17. The parameters for all computations are $h = 100$ ft, $k = 1$ s, and $\tau = 10$ s. As expected, the numerical solutions of both models are the same for initial conditions 1 and 2 (Figs. 12 and 13), which indicate that our extension of Godunov's

Table 4
Initial data for six Riemann problems

Cases	Initial density		Initial speed		Waves	
	Cells 1–75	Cells 76–150	Cells 1–75	Cells 76–150	Zhang's model	LWR model
1	50	90	$v_*(50)$	$v_*(90)$	H1	H1
2	90	50	$v_*(90)$	$v_*(50)$	R1	R1
3	50	90	$v_*(50)$	$v_*(90)-5$	H1 + H2	H1
4	50	90	$v_*(50)$	$v_*(90)+5$	H1 + R2	H1
5	90	50	$v_*(90)+5$	$v_*(50)$	R1 + H2	R1
6	90	50	$v_*(90)-5$	$v_*(50)$	R1 + R2	R1

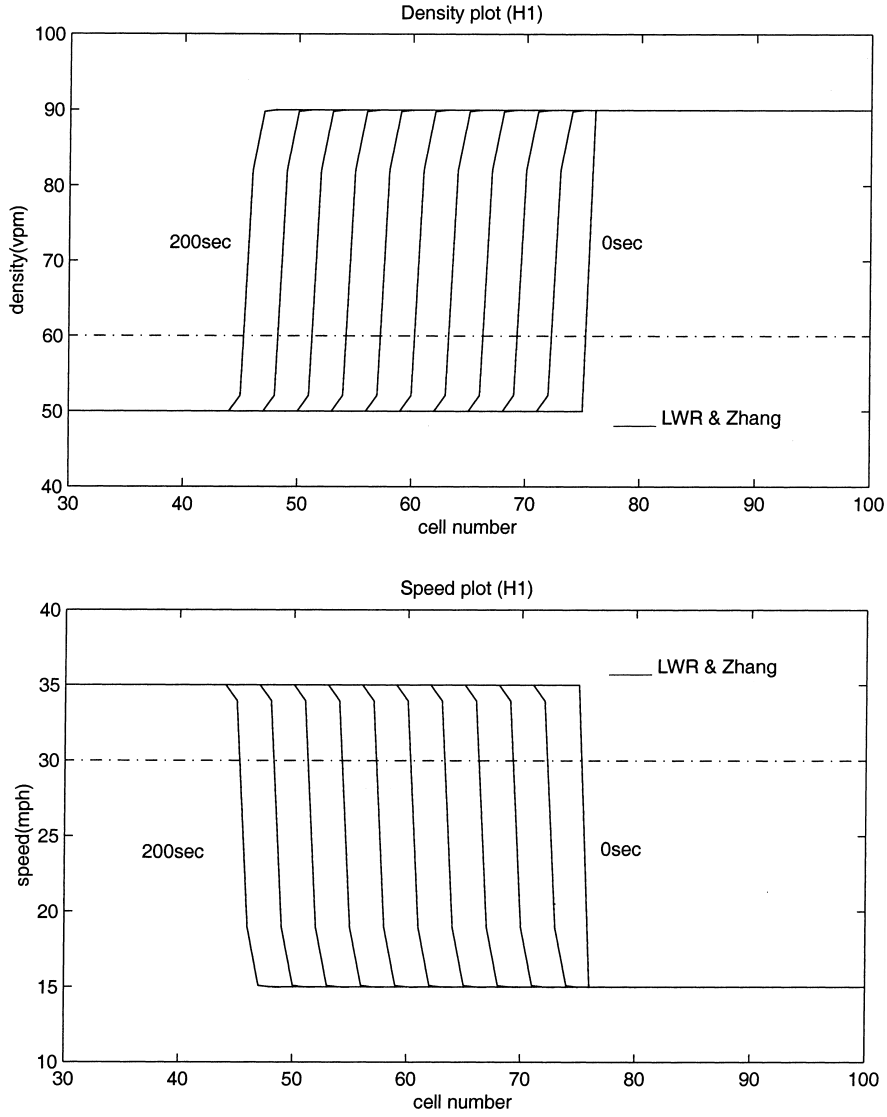

Fig. 12. Density and speed profiles, Case 1.

scheme to systems is correct. The remaining figures clearly show the effects of 2-waves (i.e., 2-shocks and 2-rarefactions) and relaxation on traffic flow. Because of the existence of 2-waves, 1-shocks in Zhang's model travel at different speeds than its corresponding shocks in the LWR model (Figs. 14 and 15). But as time increases, the speed of 1-shocks in Zhang's model approaches those of the LWR model, and so are the densities and speeds (Figs. 14–17). The difference in the speeds of 1-shocks and LWR shocks can be explained with the help of (ρ, v) and (ρ, f_*) graphs as shown in Fig. 18. This figure depicts the case of a 1-shock/2-shock combination with initial states $U_{l,r} = (\rho_{l,r}, v_{l,r})$ for Zhang's model, and a LWR shock with initial

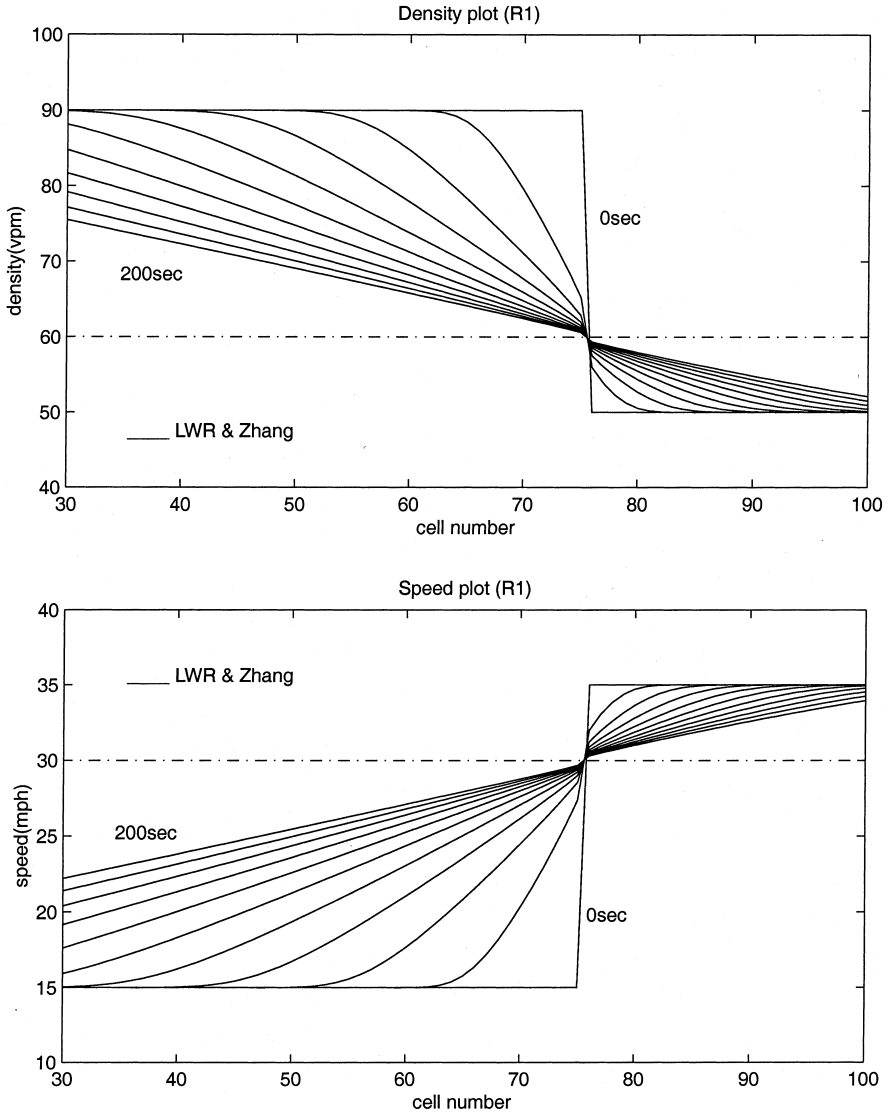

Fig. 13. Density and speed profiles, Case 2.

states $U_{*l,r} = (\rho_{l,r}, v_*(\rho_{l,r}))$ for the LWR model. The 1-shock connects states U_l and U_m and the 2-shock connects U_m and U_r, while the LWR shock connects states U_{*l} and U_{*r} . The speed of the 1-shock in Zhang's model is the slope of line LM on the (ρ, f_*) graph while the speed of the LWR shock is the slope of line LF. In this case, the 1-shock travels faster than the LWR shock. Because of relaxation, however, the state U_m is moving to state U_{*r} – an equilibrium state – as time increases, and the point M is moving to point F on the (ρ, f_*) graph, that is, the speed of the 1-shock will approach the speed of the LWR shock with the increase of time. The case of 1-shock/2-rarefaction can be similarly explained. Finally, it is also worth mentioning that in

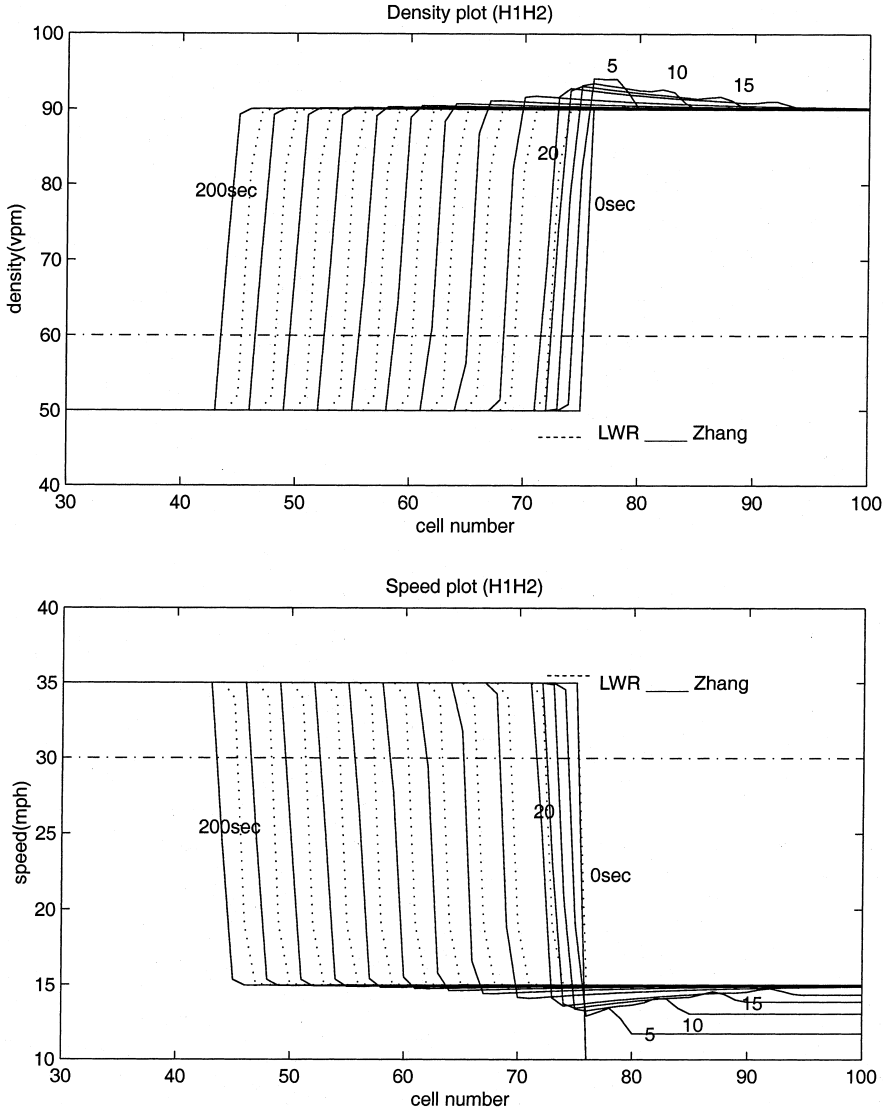

Fig. 14. Density and speed profiles, Case 3.

Zhang's model 1-shocks and 1-rarefactions are persistent and dominant while 2-shocks and 2-rarefactions are transitory.

7. Discussions

Hoping to capture the interactions among drivers as manifested through temporal and spatial evolutions of macroscopic traffic indicators such as density, speed and flow, transportation researchers often use partial differential equation(s) to describe traffic flow. These PDEs, as in the

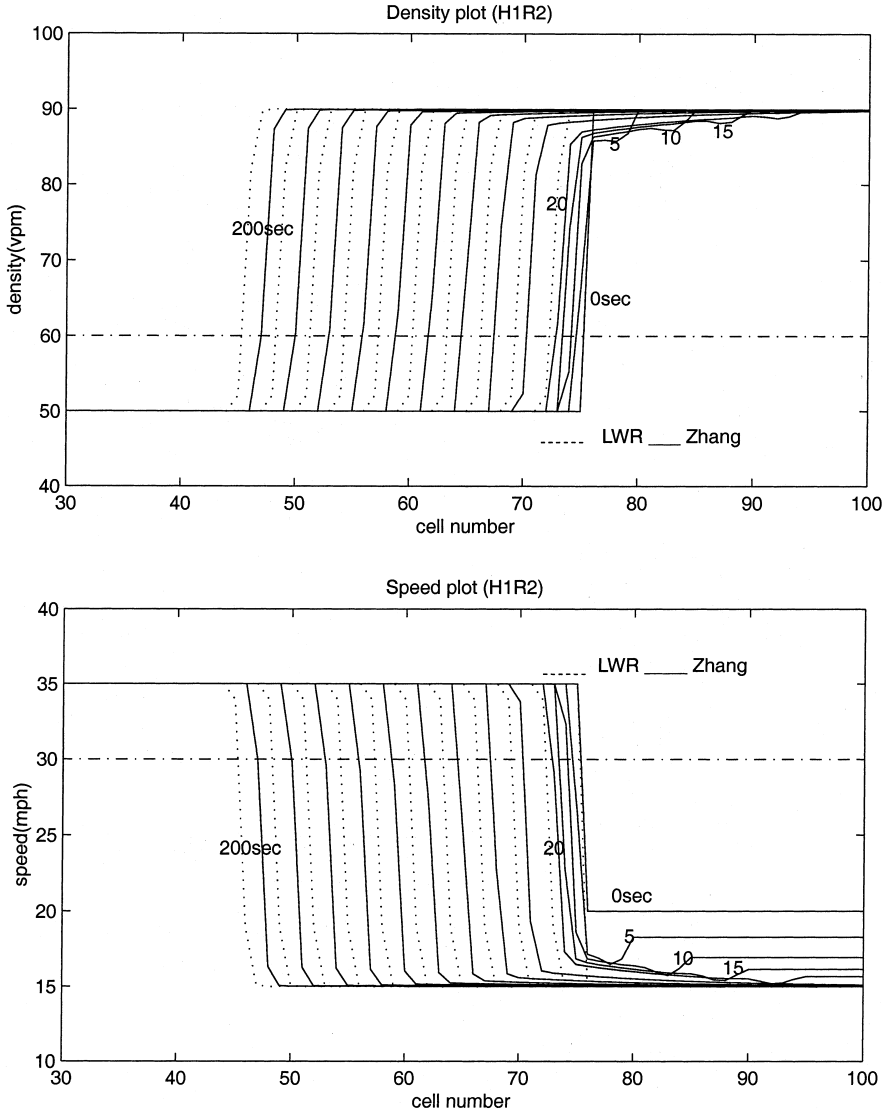

Fig. 15. Density and speed profiles, Case 4.

scalar LWR model or the two-dimensional non-equilibrium traffic flow model, are generally of hyperbolic type, in which information is propagated along certain directions (characteristic directions) at certain speeds (characteristic velocities), and could be absorbed or generated by singularities to form shock or rarefaction waves. The directional propagation of information and the existence of singularities in hyperbolic PDEs present a unique challenge to the development of finite difference approximations for such PDEs. Many seemingly reasonable finite difference approximations lead to erroneous results. Examples of such FDEs abound in literature: for example, the numerical lock-up of the LWR model reported by Ross (1988) is attributable to an inappropriate FDE, and the FDE of FREFLOW is partially to blame for the difficulties described in

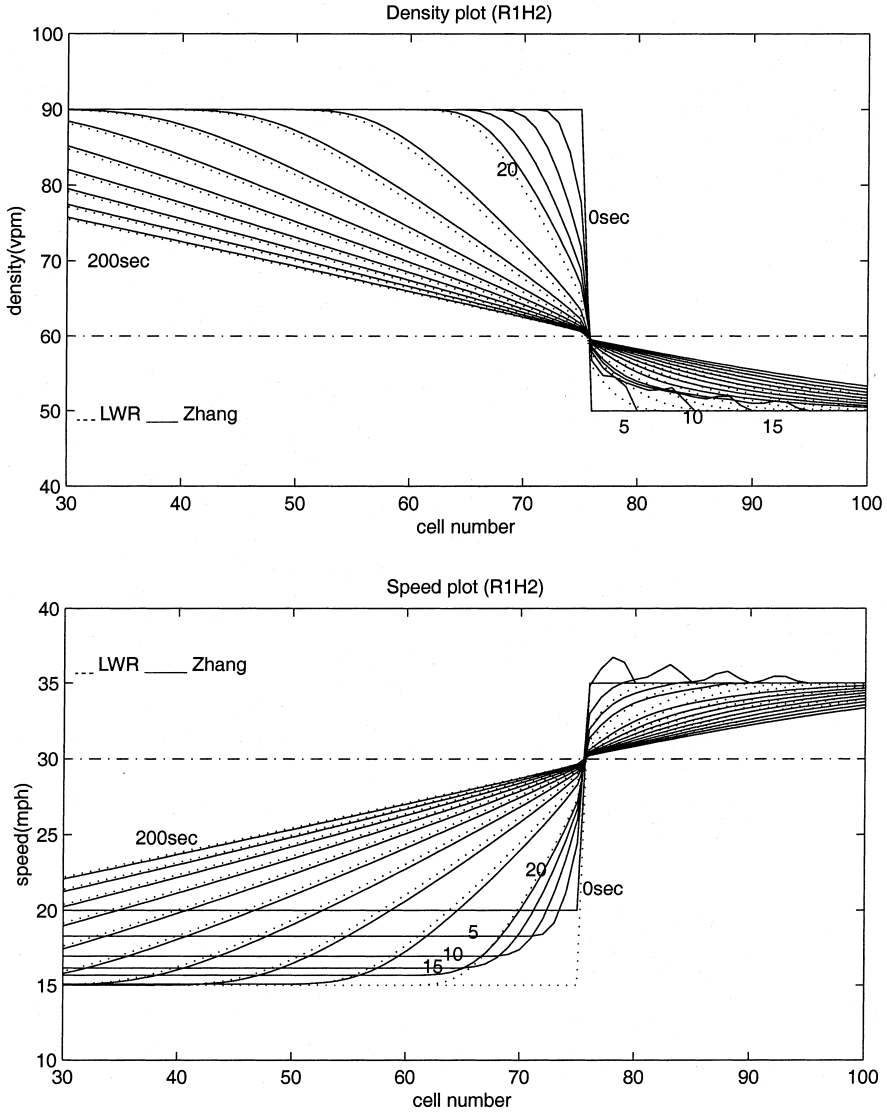

Fig. 16. Density and speed profiles, Case 5.

Derzko et al. (1983). [6] In the presence of shocks, rarefactions, and multiple solutions, special care is warranted when developing finite difference schemes to approximate hyperbolic PDEs.

A FDE, if it satisfies certain properties, has a better chance of success in approximating hyperbolic PDEs. These properties, including consistency, stability and conservativeness, usually

[6] Problems mentioned in both articles are not present when the corresponding PDEs are approximated by correct FDEs, the Murman scheme in the LWR case and an approximate Riemann solver in the PW case (Leo and Pretty, 1992).

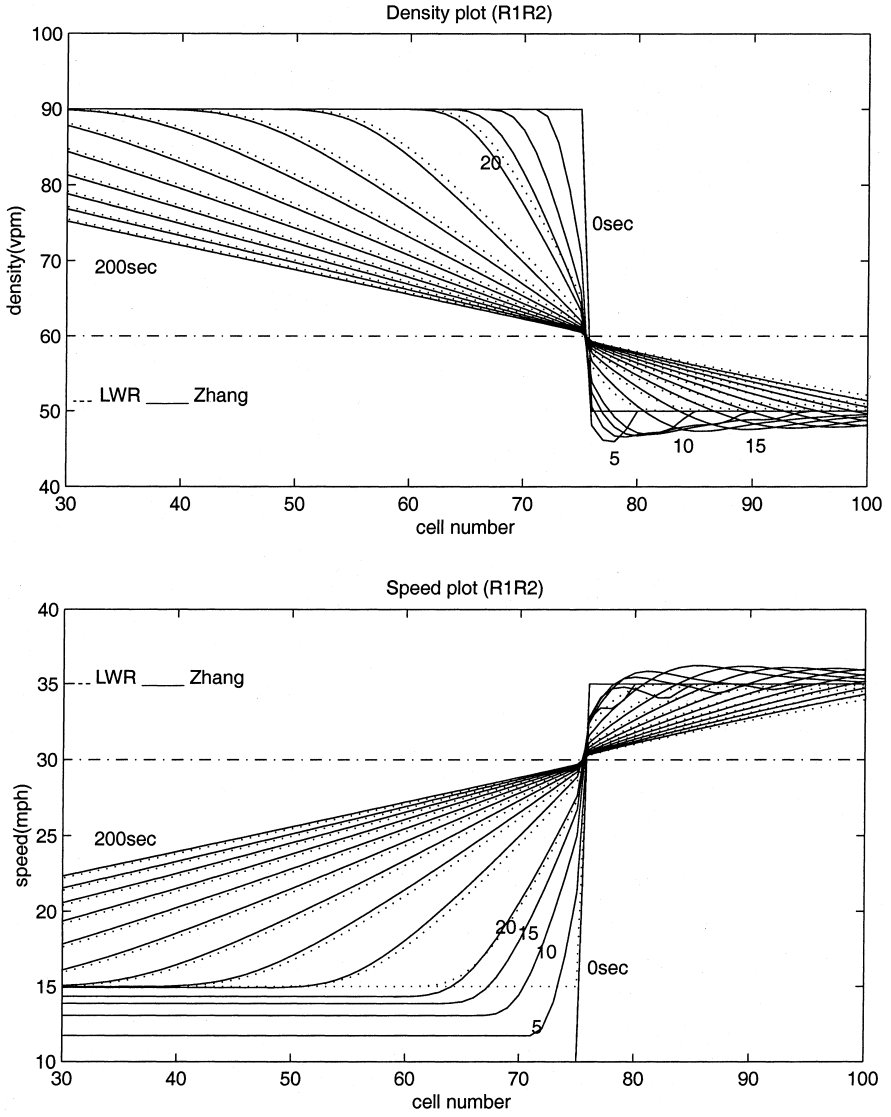

Fig. 17. Density and speed profiles, Case 6.

guarantee that the solution of the FDE converges to the correct weak solution of the PDE. One attractive way to construct such a FDE is proposed by Godunov, in which one solves a series of Riemann problems at each cell boundary for a time interval, then piece these exact solutions together to obtain new initial data for the Riemann problems of next time interval. This scheme, which has been successfully applied to solve the LWR model, is extended to solve a systems of PDEs of a non-equilibrium traffic model in this paper. In our presentation of the scheme, we not only showed how to construct such a FDE, but also pointed out the link between various Godunov-type FDEs for the LWR model and the FDE developed herein for the non-equilibrium model. Moreover, we have corrected an ambiguity inherent in the specification of boundary

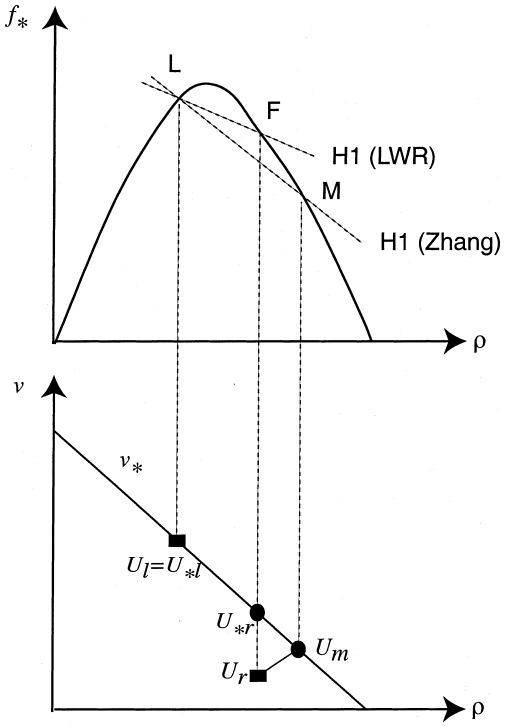

Fig. 18. Explanation of different shock speeds in Zhang's model and LWR model.

conditions using flux by imposing boundary conditions with state variables. Using the finite difference scheme, we computed numerical solutions for six Riemann problems. We found that these numerical results corroborate the theoretical analyses of Zhang (1999b).

The developed finite difference scheme provides an effective tool to simulate traffic flow and to study the behavior of higher-order continuum traffic flow models under complex initial/boundary conditions. In our further work, we plan to utilize this difference scheme in the study of non-equilibrium phase transitions in higher-order models, extend it to model bottleneck flow, and apply this scheme to the optimal control of freeway traffic.

Acknowledgements

The author wishes to thank T. Kim, graduate student of Civil and Environmental Engineering at University of California at Davis, for producing the numerical results presented in Section 6. He is also grateful to two anonymous referees for their suggestions to improve the paper.

References

Bui, D., Nelson, P., Narasimhan, S.L., 1992. Computational realizations of the entropy condition in modeling congested traffic flow, Technical Report, Texas Transportation Research Institute.

Courant, R., Friedrichs, K.O., 1948. Supersonic flow and shock waves. Interscience, New York.
Daganzo, C.F., 1995. A finite difference approximation of the kinematic wave model of traffic flow. Transportation Research B 29 (4), 261–276.
Derzko, N.A., Ugge, A.J., Case, E.R., 1983. Evaluation of dynamic freeway flow model by using field data. Transportation Research Record 905, 52–60.
Lax, P.D., 1972. Hyperbolic systems of conservations laws and the mathematical theory of shock waves. In: Society for Industrial and Applied Mathematics, Philadelphia, Pennsylvania.
Lebacque, J.P., 1996. The Godunov scheme and what it means for first order traffic flow models. In: Proceedings of the Thirteenth International Symposium on Transportation and Traffic Theory.
Leo, C.J., Pretty, R.L., 1992. Numerical simulation of macroscopic continuum traffic models. Transportation Research B 26 (3), 207–220.
LeVeque, R., 1992. Numerical Methods for Conservation Laws. Birkhäuser, Stuttgart.
Lighthill, M.J., Whitham, G.B., 1955. On kinematic waves: II. A theory of traffic flow on long crowded roads. In: Proceedings of the Royal Society, vol. A 229 (1178), pp. 317–345.
Michalopoulos, P.G., Beskos, D.E., Lin, J.K., 1984. Analysis of interrupted traffic flow by finite difference methods. Transportation Research B 18, 377–396.
Payne, H.J., 1971. Models of freeway traffic and control. In: Bekey, G.A. (Ed.), Mathematical Models of Public Systems, Simulation Councils Proc. Ser., vol. 1, pp. 51–60.
Payne, H.J., 1979. FREFLOW: A macroscopic simulation model of freeway traffic. Transportation Research Record 722, 68–77.
Richards, P.I., 1956. Shock waves on the highway. Operations Research 4, 42–51.
Ross, P., 1988. Traffic dynamics. Transportation Research B 22 (6), 421–435.
Whitham, G.B., 1974. Linear and nonlinear waves. Wiley, New York.
Zhang, H.M., 1998. A theory of nonequilibrium traffic flow. Transportation Research B 32 (7), 485–498.
Zhang, H.M., 1999. Analysis of the stability and wave properties of a nonequilibrium traffic flow. Transportation Research B 33 (6), 387–398.
Zhang, H.M., 1999b. Structural properties of solutions arising from a nonequilibrium traffic flow theory. Transportation Research B 34 (7), 583–603.